





# Detecting telecom single photons with $(99.5^{+0.5}_{-2.07})\%$ system detection efficiency and high time resolution

Cite as: APL Photonics 6, 036114 (2021); <https://doi.org/10.1063/5.0039772>

Submitted: 06 December 2020 . Accepted: 01 March 2021 . Published Online: 30 March 2021

 J. Chang, J. W. N. Los, J. O. Tenorio-Pearl, N. Noordzij,  R. Gourgues,  A. Guardiani, J. R. Zichi, S. F. Pereira, H. P. Urbach,  V. Zwiller, S. N. Dorenbos, and  I. Esmail Zadeh

## COLLECTIONS

 This paper was selected as an Editor's Pick



View Online



Export Citation



CrossMark

APL Photonics

SPECIAL TOPIC:

Photonics and AI in Information Technologies

# Detecting telecom single photons with $(99.5_{-2.07}^{+0.5})\%$ system detection efficiency and high time resolution

Cite as: APL Photon. 6, 036114 (2021); doi: 10.1063/5.0039772

Submitted: 6 December 2020 • Accepted: 1 March 2021 •

Published Online: 30 March 2021



J. Chang,<sup>1,2,a)</sup>  J. W. N. Los,<sup>2</sup> J. O. Tenorio-Pearl,<sup>2</sup> N. Noordzij,<sup>2</sup> R. Gourgues,<sup>2</sup>  A. Guardiani,<sup>2</sup>  J. R. Zichi,<sup>3</sup> S. F. Pereira,<sup>1</sup> H. P. Urbach,<sup>1</sup> V. Zwiller,<sup>2,3</sup>  S. N. Dorenbos,<sup>2</sup> and I. Esmaeil Zadeh<sup>1,2</sup> 

## AFFILIATIONS

<sup>1</sup>Optics Research Group, ImPhys Department, Faculty of Applied Sciences, Delft University of Technology, Delft 2628 CJ, The Netherlands

<sup>2</sup>Single Quantum B.V., Delft 2628 CJ, The Netherlands

<sup>3</sup>Department of Applied Physics, KTH Royal Institute of Technology, Albanova University Centre, Roslagstullsbacken 21, 106 91 Stockholm, Sweden

<sup>a)</sup>Author to whom correspondence should be addressed: [j.chang-1@tudelft.nl](mailto:j.chang-1@tudelft.nl)

## ABSTRACT

Single photon detectors are indispensable tools in optics, from fundamental measurements to quantum information processing. The ability of superconducting nanowire single photon detectors (SNSPDs) to detect single photons with unprecedented efficiency, short dead time, and high time resolution over a large frequency range enabled major advances in quantum optics. However, combining near-unity system detection efficiency (SDE) with high timing performance remains an outstanding challenge. In this work, we fabricated novel SNSPDs on membranes with  $(99.5_{-2.07}^{+0.5})\%$  SDE at 1350 nm with 32 ps timing jitter (using a room-temperature amplifier), and other detectors in the same batch showed 94%–98% SDE at 1260–1625 nm with 15–26 ps timing jitter (using cryogenic amplifiers). The SiO<sub>2</sub>/Au membrane enables broadband absorption in small SNSPDs, offering high detection efficiency in combination with high timing performance. With low-noise cryogenic amplifiers operated in the same cryostat, our efficient detectors reach a timing jitter in the range of 15–26 ps. We discuss the prime challenges in optical design, device fabrication, and accurate and reliable detection efficiency measurements to achieve high performance single photon detection. As a result, the fast developing fields of quantum information science, quantum metrology, infrared imaging, and quantum networks will greatly benefit from this far-reaching quantum detection technology.

© 2021 Author(s). All article content, except where otherwise noted, is licensed under a Creative Commons Attribution (CC BY) license (<http://creativecommons.org/licenses/by/4.0/>). <https://doi.org/10.1063/5.0039772>

## INTRODUCTION

A single photon stands for the quantum excitation of electromagnetic radiation. Driven by the explosive growth of quantum information science<sup>1</sup> and quantum computation technology<sup>2</sup> in the past few decades, technologies with regard to processing light at the single photon level have been greatly explored and developed.<sup>3</sup> In the single photon detection end, avalanche photon diodes (APDs) are widely used due to their wide detection spectrum range, tunable detection speed, and non-cryogenic operation temperature.<sup>4</sup> Since APDs' response to infrared photons is typically lower compared to visible photons, frequency upconversion

detectors can be used to solve this problem by upconverting the telecom wavelength of photons to the visible wavelength<sup>5</sup> for easier detection. However, both APDs and frequency upconversion detectors have limited system detection efficiency (SDE), especially in the infrared region. Superconducting nanowire single photon detectors (SNSPDs) emerged as a key technology for quantum optics experiments and photonic applications over the last two decades.<sup>3,6,7</sup> Achieving unity system detection efficiency with SNSPDs has been a long-standing, promising yet challenging goal. It will largely benefit various applications; for example, in quantum key distribution (QKD) systems,<sup>8–10</sup> single photon detectors with high efficiency are essential for receiving secured quantum keys over long

distances. High-efficiency detectors also allow for closing loopholes and certify that a quantum communication scheme based on entanglement is secure.<sup>11</sup> In addition, for experiments requiring coincidence measurements in multiple detectors, near-unity detection efficiency is required for each channel because the multi-photon count rate depends on the efficiency product of detectors involved. For example, the 12-photon coincidence count rate<sup>12</sup> is about 1/h with detectors of 75% efficiency. For the same measurement, if detectors with 99.5% efficiency could be used, the coincidence count rate would be increased to 1 per two minutes. Similarly, in boson sampling, single photon detectors with high SDE are required in ambitious experiments, aiming for quantum supremacy.<sup>13</sup> Besides near-unity system efficiency, high timing performance is crucial for applications where photon arrival time is required to be precisely recorded. For example, in high-dimensional QKD,<sup>14,15</sup> multiple bits per photon pair can be realized by encoding information on the photons' arrival times, and thus, both high efficiency and time resolution are required. Similarly, high timing performance is essential for improving depth resolution in light detection and ranging,<sup>16,17</sup> distinguishing a signal from false counts in dark matter detection,<sup>18</sup> enhancing the quality of quantum imaging systems,<sup>19,20</sup> and making photons with a small energy difference indistinguishable for quantum erasure application.<sup>21</sup> More radically, the fast-expanding quantum technologies in recent years are based on quantum states that violate local realism, as shown in Refs. 22 and 23, and high performance SNSPDs have played important roles in experiments that successfully demonstrated loophole-free violation of Bell's inequalities.

With demands from emerging applications and the quest to understand SNSPDs' detection limits, efforts were made in the past years to improve SDE toward unity.<sup>24–29</sup> As summarized in Table I, different material platforms were developed to achieve the highest SDE. However, achieving unity efficiency simultaneously with ultrahigh time resolution remains a challenge. Here, using a 9 nm thick NbTiN superconducting film made by an optimized magnetron co-sputtering deposition process<sup>30</sup> and a membrane cavity, we fabricated SNSPDs with over 99% SDE at 1350 nm (also over 98% SDE at 1425 nm; see the section titled “List of measured devices” of the supplementary material) and above 94% efficiency in the wavelength range of 1280–1500 nm. These detectors also achieved 15–26 ps timing jitter with a cryogenic amplification readout circuitry and an electrical recovery time of about 33 ns (1/e recovery time). Additionally, we explicitly clarify SNSPDs' efficiency measurement pitfalls and requirements, which will be a solid reference for single photon applications and characterization of single photon detectors.

## OPTICAL SIMULATION AND DEVICE DESIGN

Typically, SNSPDs are meandering superconducting nanowires embedded in an optical cavity. An optimized optical cavity and a meandered nanowire design are indispensable to achieve high system detection efficiency. Recently, works from two different groups showed Distributed Bragg Reflectors (DBRs) integrated with SNSPDs with ~98% SDE.<sup>28,29</sup> In Ref. 28, SNSPDs made from a twin-layer NbN nanowire on the DBR (13 alternative SiO<sub>2</sub>/Ta<sub>2</sub>O<sub>5</sub> layers) showed 95% efficiency at 1550 nm (2.1 K) and 98% efficiency at 1590 nm (0.8 K). The sandwich structure (NbN/SiO<sub>2</sub>/NbN, 6/3/6 nm) enabled simultaneous high optical absorption and saturated internal efficiency, and thus, high SDE was achieved. Another work<sup>29</sup> demonstrated that SNSPDs made from 4.1 nm MoSi on the DBR (13 layers of  $\alpha$ -Si/SiO<sub>2</sub>) showed 98% SDE at 1550 nm (0.7 K). Therefore, high SDE was achieved by employing amorphous MoSi with strong saturated internal efficiency, using the optimized DBR, and adding fiber spacers. Since both works employed a thick DBR cavity (a few  $\mu$ m), light divergence is high after bouncing several times inside the cavity stacks; thus, bigger detectors (23–50  $\mu$ m diameter) are needed for good optical absorption.<sup>29</sup> However, larger SNSPDs lead to high kinetic inductance, slower recovery, low yield, and higher jitter. Especially for NbTiN-based large detectors, the nature of the polycrystalline materials<sup>30</sup> degrades the performance because of higher film inhomogeneity compared to amorphous materials.<sup>31</sup> In order to overcome this challenge, our work employed a thinner SiO<sub>2</sub>/Au membrane cavity (~230/150 nm), and it has less beam divergence compared to thick DBR stacks. However, achieving very high optical absorption efficiency in detector layer puts stringent requirements on the metal reflector. By using thermal evaporation, we fabricated gold mirror with ultrahigh reflection (98–99%, see supplementary section S3.2). Such a high reflection metal mirror allowed us to fabricate smaller SNSPDs with high SDE (94%–99.5%) and high time resolution (15–26 ps) simultaneously. Based on the above-mentioned discussion, we made two different meandered nanowire designs: 50/120 nm and 70/140 nm (linewidth/pitch). Both designs have a radius of 8  $\mu$ m so that our device diameter is 30%–70% smaller than in recently reported high SDE works.<sup>28,29</sup> The top panel in Fig. 1(a) illustrates the NbTiN nanowire supported by a SiO<sub>2</sub>/Au membrane, and the bottom panel shows an optical microscope image of the meandered nanowire on a SiO<sub>2</sub> membrane before (left) and after (right) deposition of a Au reflector. This compact optical cavity design allows us to make smaller meandered nanowires without degrading the SDE. In addition, a smaller device leads to lower kinetic inductance, translating into a faster detection signal rising edge and better timing performance.<sup>32–35</sup>

**TABLE I.** Comparison of different high-efficiency SNSPDs.

Material/temperature	SDE jitter	Wavelength (nm)	Reference
WSi/120 mK	93%/150 ps	1550	24
NbN/1.8–2.1 K	90%–92%/79 ps	1550	25
NbTiN/2.5 K	92%/14.8 ps	1310	26
MoSi/700 mK	95%/unknown	1520–1550	27
MoSi/700 mK	98%/unknown	1550	29
NbN/800 mK–2.1 K	95%–98%/65.8–106 ps	1530–1630	28
NbTiN/2.5–2.8 K	94%–99.5%/15.1 ps	1290–1500	This work

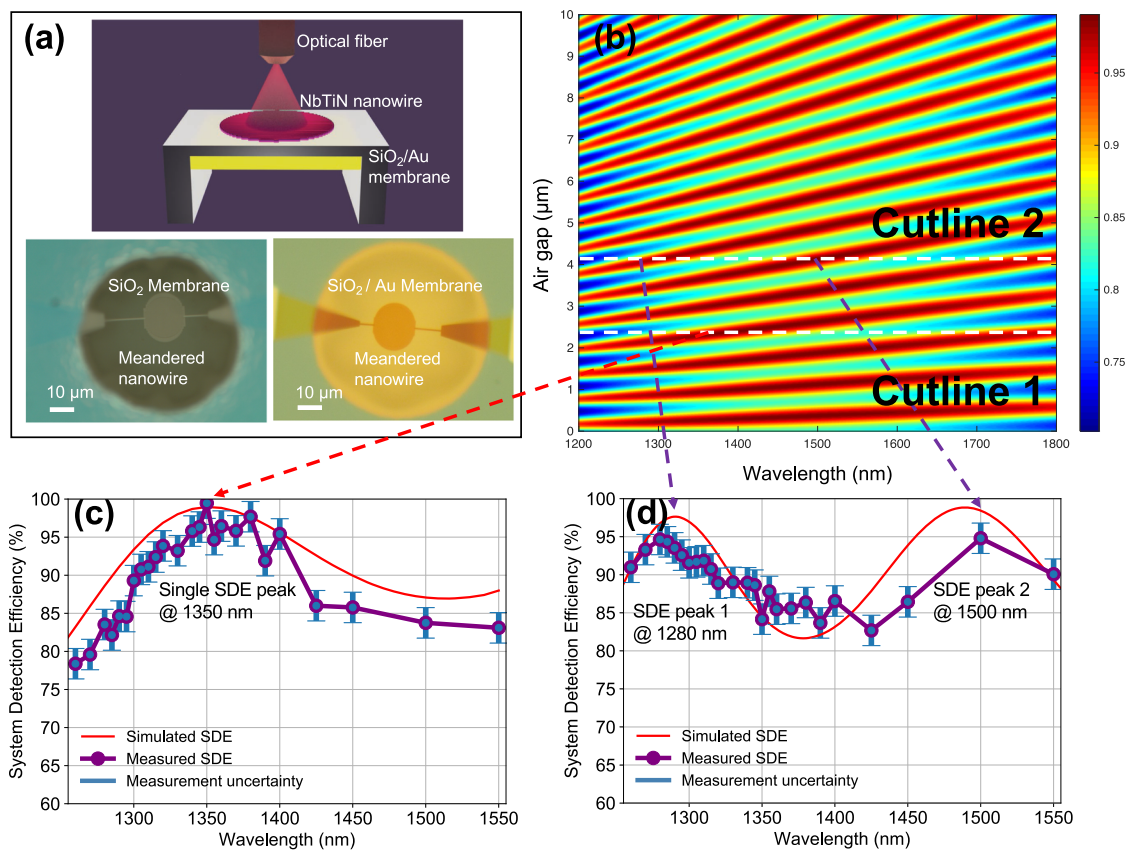


**FIG. 1.** (a) Top panel illustrates the device structure of the meandered nanowire on a  $\text{SiO}_2/\text{Au}$  membrane, and the bottom panel shows an optical image of the meandered nanowire on a  $\text{SiO}_2$  membrane before/after (left/right) Au deposition. (b) Simulated optical absorption for a device with a 0–10  $\mu\text{m}$  air gap. Cutline 1 shows that when the air gap is around 2.2  $\mu\text{m}$ , only one SDE peak occurs around 1350 nm, and cutline 2 shows that with an air gap of 4.1  $\mu\text{m}$ , two SDE peaks are obtained. (c) Measurement and simulation of detector #1 with SDE over 99% at 1350 nm. (d) Measurement and simulation of detector #2 with dual peaks at 1280 nm and 1500 nm, both exceeding 94% SDE.

In addition, our NbTiN-based detectors are operated in a 2.5–2.8 K Gifford–McMahon cryo-cooler; compared to Refs. 28 and 29, the cryostat in our work is simpler, cost-effective, and more compact.

To achieve an efficient optical fiber to detector coupling, we used the ferrule–sleeve method described in Ref. 26. The air gap between the detector and the fiber plays an important role in total optical absorption. The air gap is defined by multiple sources: (i) fabrication residuals left around the device or dust on the fiber end surface, (ii) Au contacts around the detector, and (iii) the potential drift of the fiber core during cooling/warming, leaving a gap between the detector and the fiber. In this work, finite-difference time-domain (FDTD) simulations were carried out for a systematic study of optical absorption. As shown in Fig. 1(b), when the air gap is around 2.2  $\mu\text{m}$ , only one efficiency peak can be observed along cutline 1. As a result, Fig. 1(c) shows simulation and measurement results of detector #1 with >99% SDE at 1350 nm. With the increase in the air gap distance, more complex absorption situations are obtained. For example, along cutline 2, dual absorption peaks are expected. We point out that an air gap does not always reduce absorption. With proper control of the air gap, one could achieve maximum absorption at selected wavelengths. As a direct demonstration, Fig. 1(d) shows simulation and measurements of detector #2 with two SDE

peaks at 1280 nm and 1500 nm. Both SDEs exceed 94% similar to the previously reported more complex cavities,<sup>36</sup> and the controlled design of such detectors would benefit applications where multiple wavelengths must be efficiently detected simultaneously.

## DEVICE FABRICATION

Based on the simulation results, device fabrication was carried out as described below. Initially, a 230 nm thick  $\text{SiO}_2$  layer was grown by thermal oxidation on a commercial Si wafer. On top of the  $\text{SiO}_2$  layer, a NbTiN thin film was deposited by co-sputtering of Nb and Ti in a plasma of Ar and  $\text{N}_2$ , as described in Ref. 30. The meandering nanowire structure was then written by electron beam lithography with either HSQ (first batch, negative) or AR-P 6200.04 (second batch, positive) E-beam resist. After development, the nanowire pattern was transferred to the NbTiN layer by reactive ion etching with mixed gases of  $\text{SF}_6$  and  $\text{O}_2$ . Afterward, using deep reactive ion etching and metal evaporation, we fabricated a thin  $\text{SiO}_2$  membrane with a Au mirror beneath the NbTiN nanowire, as described in the section titled “Device Fabrication” of the [supplementary material](#). Finally, a deep silicon etch step (Bosch etching) released the detectors.

## EFFICIENCY MEASUREMENT SETUP

Prior to any measurement, the laser was turned on for  $>1$  h for power stabilization. Every optical component including fibers was fixed to avoid the influence from mechanical vibration and air turbulence. We used the following two-step procedure to carry out system efficiency measurements: (i) Building an accurate laser attenuator. Initially, the continuous-wave (CW) laser beam passes through the first fiber-to-fiber coupler (FBC-1550-FC, containing a polarizer) followed by a fiber-coupled beam splitter (with a splitting ratio of 99–1). The high power branch is recorded by using an optical powermeter  $P_1$ , while the low power branch is directed toward the second fiber-to-fiber coupler (containing neutral density filters and a polarizer) and a polarization controller. Similarly, the power after the polarization controller is recorded with an optical powermeter  $P_2$ . By adjusting polarizers in both fiber-to-fiber couplers and choosing the proper neutral density filters, we set the power ratio  $P_1/P_2$  to the desired values (50–60 dB). After the attenuation ratio was set, all components were kept fixed. (ii) Controlling precisely the input photon flux. We lowered the input power by adding extra neutral density filters before passing through the first polarizer to lower  $P_1$  to 1–10 nW. We also rechecked the attenuation ratio multiple times before and after the measurements to assure nothing has been changed in the setup (see the section titled “Efficiency measurement stability” of the [supplementary material](#)). After this two-step procedure, different input photon fluxes can be set up; for example, 10 nW with 50 dB attenuation corresponds to 679k photons/s at 1350 nm.

It must be noted that to avoid fiber-to-fiber coupling losses when connecting to the detection system, we preselected the fibers that have the best coupling match to the fibers inside our cryostat. Finally, the fiber at the output of the polarization controller was connected to the pre-selected fiber and then guides light into the system for measurements.

Our SDE was calculated as  $\eta_{SDE} = (1 - R_{\text{ref}}) \cdot (N_{\text{count}}/N_{\text{total}})$ , where  $N_{\text{count}}$  is the total registered count rate by our system and  $N_{\text{total}}$  is the total input photon number.  $R_{\text{ref}}$  is added to avoid overestimation of the SDE, and it represents the simulated and measured fiber–air interface reflection (see the section titled “Fiber end-face reflection” of the [supplementary material](#)). Since the total input photon flux was calculated by  $N_{\text{total}} = P \cdot \lambda / (hc)$ , where  $P$  is the measured optical power,  $h$  is the plank constant,  $c$  is the speed of light in vacuum, and  $\lambda$  is the used wavelength, we carefully evaluate our laser spectrum with an optical spectrum analyzer. In [Fig. 2\(b\)](#), we show the measured spectrum of the tunable laser at variable wavelengths, from 1290 to 1650 nm. As a result, [Fig. 2\(c\)](#) demonstrates that the laser has a linewidth of  $<1$  nm. The slight shift of the measured wavelength with the set value is mainly due to the optical spectrum analyzer’s calibration, which has a negligible influence on our SDE measurement. For input power measurement, accurate optical powermeters are necessary. As shown in [Fig. 2\(d\)](#), readings of four different optical powermeters at 1350 nm are presented with their uncertainties. All readings are normalized to the Newport IG-818-L (used for our measurements) since it has 2%

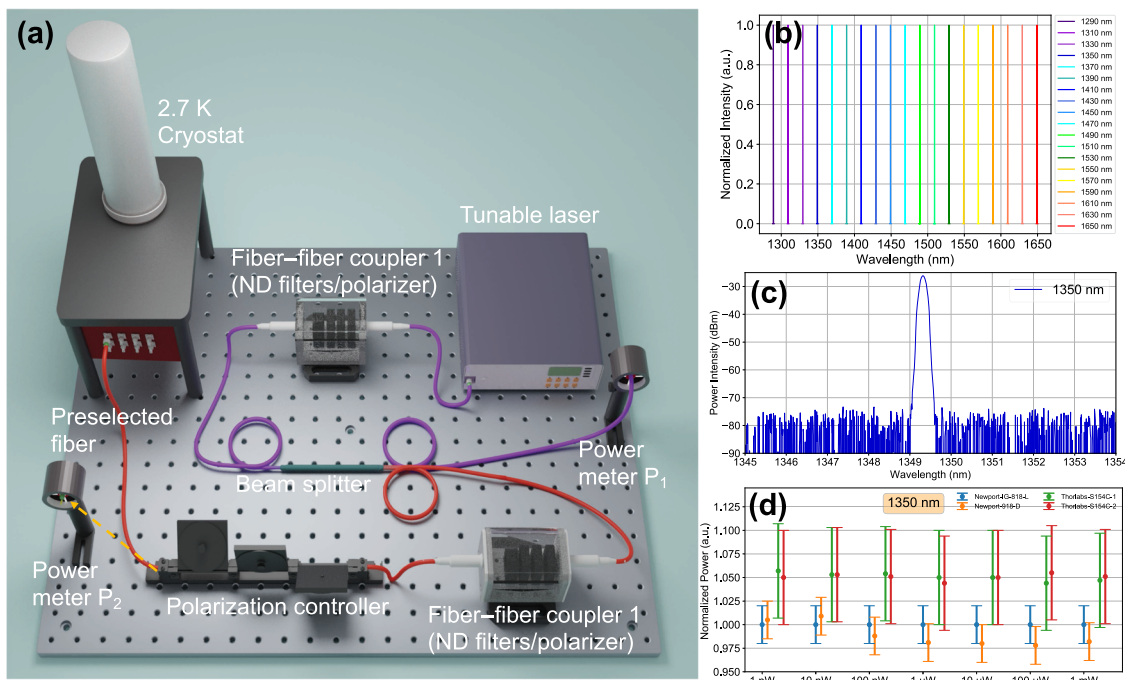


**FIG. 2.** (a) System detection efficiency measurement setup. Emission from a tunable laser passes a bench containing neutral density (ND) filters and a polarizer and goes through a 99–1 fiber-coupled beam splitter to split the signal toward powermeter  $P_1$  (99%) and powermeter  $P_2$  (1%). (b) Measured spectrum of the tunable laser at 1290–1650 nm. (c) Measured laser spectrum at 1350 nm showing a laser linewidth of  $<1$  nm. (d) Readings of four different optical powermeters at 1350 nm with different error bars. All readings are normalized to the Newport IG-818-L powermeter.

accuracy from 20 pW to 10 mW and a good linearity uncertainty of 0.5%.

## DETECTION PERFORMANCE AND DISCUSSION

Prior to SDE measurements, we studied the relationship between SNSPDs' detection reset kinetics and their efficiency recovery. We performed auto-correlation measurements between two subsequent detection events with the detectors illuminated by a CW laser similar to Ref. 37. After collecting more than 50 000 events, as shown in the top panel of Fig. 3(a), we built a delay time histogram. Together with the SNSPD detection pulse shown in the bottom panel of Fig. 3(a), we can see that within the first 25 ns, no subsequent pulse can be detected; thus,  $\tau_1 = 25$  ns can be defined as the minimum separation dead time. For most SNSPD related studies,  $1/e$  dead time (time for pulse to decay from peak amplitude to  $1/e$  of the amplitude) is often used to describe the device recovery property. It can be seen that our device's  $1/e$  dead time is  $\tau_2 = 33$  ns. Furthermore,  $\tau_3 = 51$  ns represents the time when the detector recovers 50% of the maximum efficiency, also known as  $-3$  dB efficiency dead time, and  $\tau_4 = 97$  ns stands for full efficiency recovery time. These measurements indicate that the input photon flux can influence SDE because if the photon flux is too high, photons arriving within the dead times of the detector cannot be registered at the detectors' maximum efficiency; thus, an optimal input photon flux is necessary to achieve maximum detection efficiency. It must be noted that much higher photon fluxes can be achieved (with no loss of efficiency) if the source is pulsed (photons arriving with regular timings in between).<sup>26</sup>

We characterized 40 detectors in two separate fabrication rounds. As shown in Fig. 3(b), detector #1 was the best detector from the first fabrication batch and was tested at 1350 nm with different input photon fluxes. Initially, the photon flux was set to 10 nW plus 50 dB attenuation ( $\sim 679$  000 photons/s), and device #1 showed a SDE of 94%–95%. With an input photon flux below 4 nW plus 50 dB attenuation ( $\sim 271$  600 photons/s), device #1 achieved a saturated SDE of  $(99.5^{+0.5}_{-2.07})\%$ . Similarly, detector #3 from the second fabrication batch was tested at different wavelengths and showed  $>98\%$  SDE at 1425 nm, as shown in Fig. 3(c). It is worth mentioning that, as shown in Figs. 3(b) and 3(c), the dark count rate (DCR) of our detector is of the order of 300–500 Hz. We believe this value can be further reduced to below 1–10 Hz by using a cold filter<sup>38</sup> in the system or employing a fiber with end-face coatings.<sup>39</sup> For more examples, see the section titled “List of measured devices” of the [supplementary material](#).

Besides high SDE, time resolution is another crucial advantage of SNSPDs compared with other single photon detectors. The Instrument Response Function (IRF) of our detectors was characterized with a ps-pulse laser (1064 nm) and a fast oscilloscope (4 GHz bandwidth, 40 GHz sampling rate), as described in Ref. 26. As shown in Fig. 3(d), with a low-noise cryogenic amplifier mounted on a 40 K stage in the same cryostat, the IRF of device #15 shows a Gaussian shape histogram; after fitting, we obtain  $15.1 \pm 0.05$  ps (full width at half maximum, FWHM) timing jitter. This detector was measured to have more than 91% SDE, and the ultralow timing jitter was mainly achieved by fabricating relatively small detectors, which results in lower kinetic inductance and, thus, better jitter.<sup>33,34</sup> For more

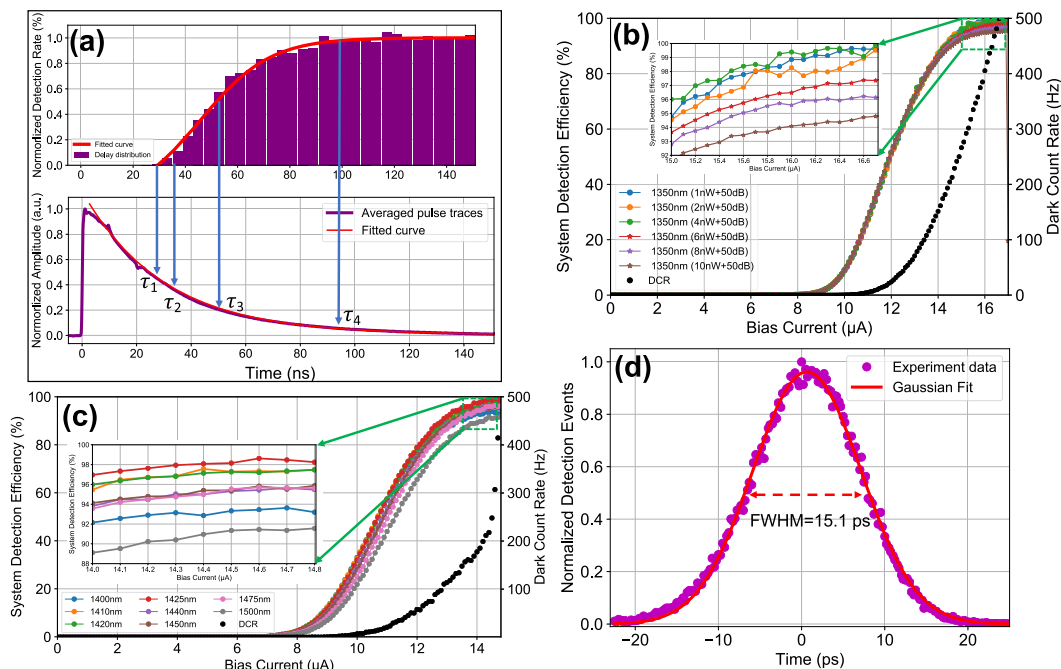


**FIG. 3.** (a) The top panel shows the auto-correlation measurement of a detector indicating SDE recovery dynamics. The bottom panel shows an averaged pulse trace from the same detector. (b) SDE measurements of detector #1 at 1350 nm with different input photon fluxes. When the input photon flux is below 4 nW plus 50 dB attenuation, the SDE of detector #2 reached  $>99\%$ , which is also shown in the inset. (c) SDE measurements of detector #3 at different wavelengths. The maximum SDE of detector #3 reached  $>98\%$  at 1425 nm. (d) Jitter measurement from a detector with  $>91\%$  SDE with a cryogenic amplifier. A Gaussian fit gives a FWHM jitter of 15.1 ps.

statistics of jitter measurement, see the section titled “Overview of tested detectors” of the [supplementary material](#). In short, we achieved 15.1–26 ps jitter with cryogenic amplifiers and 29–39 ps jitter with the room-temperature amplifier readout circuitry.

## FUTURE PERSPECTIVES ON A “PERFECT” SNSPD

Considering this work and recently published papers toward near-unity efficiency SNSPDs,<sup>28,29</sup> we would like to conclude that after nearly two decades of development since 2001,<sup>6</sup> SDE of SNSPDs has drastically improved from extremely low to approaching unity (>98%–99%). At the same time, jitter of SNSPDs has been pushed down to sub-10 ps,<sup>26</sup> which makes SNSPDs the best available technology so far for detecting single photons in a wide electromagnetic spectrum range with unprecedented timing resolution. In the coming future, in order to make a “perfect” single photon detector, we still foresee the following challenges ahead of us: (i) How to make larger SNSPDs for applications where an active area of hundreds of micrometers or even centimeter scale is needed? This requires fabricating a superconducting film with excellent uniformity and detection response and the use of large SNSPDs arrays. (ii) How to fabricate and read out a SNSPD camera with thousands or millions of pixels? This requires new designs of multipixel SNSPDs and the scalable readout circuitry. (iii) How to improve the working temperature of SNSPDs so that a more compact and inexpensive cryostat can be utilized? This requires a high-temperature superconductor material with good detection performance. (iv) How to improve the yield of high performance detectors to lower the commercial SNSPD systems’ costs? This requires better understanding of SNSPDs’ detection mechanism, employing a robust device design and fabrication recipe and high-throughput SNSPDs characterization. If the above-mentioned aspects can be realized, SNSPDs will enable more ground-breaking quantum optics applications and experiments in the near future.

## CONCLUSION

In conclusion, we demonstrated NbTiN-based SNSPDs operated at 2.7 K with high performance: our best detectors showed a SDE of  $(99.5^{+0.5}_{-2.07})\%$  at 1350 nm (time jitter of 35 ps with room-temperature amplifiers) and  $98\% \pm 2.07\%$  at 1425 nm (time jitter of 26 ps with cryogenic amplifiers). Detectors from the same batch reached SDEs above 94% (in the wavelength range of 1280–1500 nm) and sub-20 ps (best detector 15 ps) time jitter using cryogenic amplifiers. The ultrahigh efficiencies were achieved using the following methods: (i) an optimized thick NbTiN superconducting film with saturated internal efficiency, (ii) an optimized broadband membrane cavity coupled to small detectors, and (iii) accurate system efficiency measurements with a narrow linewidth tunable laser to precisely locate the high-efficiency peaks. Compared with previously reported high-efficiency SNSPDs,<sup>24,27,29</sup> our work presents a platform with higher operation temperature (2.5–2.8 K, compatible with compact closed-cycle cryostats), short recovery time, and high timing resolution. At the same time, the system efficiency performance of our devices is in par with recently reported NbN-based SNSPDs<sup>28</sup> even after using a simpler fabrication method (single-layer meander), higher operation temperature (no need for a mK cooler), and

better timing resolution. Our detectors can be further developed by considering the following aspects: (i) multiplexing the detector and controlling individual pixels by cryo-CMOS electronics to realize imaging at the single photon level, (ii) extending the detection spectrum in the mid-infrared by tailoring and optimizing NbTiN films, and (iii) improving the working temperature of the detectors with novel superconducting materials.

## METHODS

To achieve accurate SNSPD efficiency measurements, we addressed the following aspects separately.

### Optical simulation

To simulate the absorption of the optical stack, we used the commercially available FDTD Solutions software from Lumerical. The SNSPD was modeled as the cross section of a single nanowire in an optical cavity. From top to bottom, the simulated stack structure was organized as follows: an optical fiber layer (SiO<sub>2</sub>), an air gap, a NbTiN meander, a 1/4 λSiO<sub>2</sub> layer, and a 150 nm thick Au mirror. In addition, in order to check the simulation reliability, we performed transfer matrix simulation to compare and double-check with our FDTD simulation. The negligible plasmonic loss in the Au layer is also explained in detail in the section titled “Optical Simulation” of the [supplementary material](#).

### Laser source

A tunable laser (JGR-TLS5) with attenuation was employed as a quasi-single photon source. The laser covers the range of 1260–1650 nm with a step size of 0.1 nm (FWHM). For more details on the laser, see the section titled “Tunable laser source” of the [supplementary material](#). Compared with previous work,<sup>26</sup> which used photodiodes operated at a single wavelength, the tunable laser has two major advantages: First, its narrow spectrum (<1 nm) at a tuned frequency allows for precise measurements and second, a laser with a tunable wavelength enabled mapping system efficiency at different wavelengths. In this way, we precisely determined the peak efficiency and built the spectral response.

### Optical powermeters

A semiconductor-based optical powermeter was the key reference for efficiency measurements. In this work, we used two different types of powermeters: Thorlabs S154C (NIST traceable, ±5% uncertainty) and Newport 818-IG-L (NIST traceable, ±2% uncertainty). However, for the measurement, one should not only take the powermeter accuracy into consideration but should also consider sensor linearity, spectral range, power range, stability, and all other related parameters. For details, see the section titled “Optical power meters” of the [supplementary material](#).

### Measurement uncertainty calculation

For system detection efficiency measurement uncertainty, we considered all possible uncertainties in our experiments and calculated the total measurement uncertainty with the root-mean-square (rms) of the sum of the squared errors. The uncertainties in our measurements include the powermeter measurement uncertainty (2%),

linearity uncertainty (0.5%), laser stability uncertainty (<0.1%), and optical attenuator uncertainty (<0.2%). For detailed measurement uncertainty calculations, see the sections titled “Efficiency measurement stability” and “Measurement uncertainty” of the [supplementary material](#). In short, our efficiency measurement has a total uncertainty of  $\pm 2.07\%$  (rms).

### Fiber end-face reflection

When measuring laser power within the fiber with a powermeter, the fiber end-facet was not in direct contact with the powermeter’s sensor. The existing fiber-to-air interface leads to a reflection of up to a few percent back toward the light source.<sup>26</sup> On the other hand, physical contact polished fiber-to-fiber connections have negligible back reflections (typically  $-30$  to  $-40$  dB). For all our efficiency measurements, we removed this back reflection contribution by multiplying a correction factor of  $(1-R_{\text{ref}})$ . To determine the accurate value of  $R_{\text{ref}}$ , see the section titled “Fiber end-face reflection” of the [supplementary material](#).

### Polarization degree

Since our detectors were patterned along meandering shapes, light absorption can be significantly different based on the light polarization direction along the meander’s direction.<sup>40</sup> Thus, it is important to have a linearly polarized input light and fully control the polarization. In the section titled “Polarization degree and control” of the [supplementary material](#), we show detailed measurement of degree of linearity and polarization control.

### AUTHORS’ CONTRIBUTIONS

J.C. and J.W.N.L. contributed equally to this work.

### SUPPLEMENTARY MATERIALS

See the [supplementary material](#) for complete details of the list of measured devices (S1), device fabrication (S2), optical simulation (S3), the tunable laser source (S4), optical powermeters (S5), efficiency measurement stability (S6), measurement uncertainty (S7), fiber end-face reflection (S8), polarization degree and polarization control (S9), and electronic counting circuitry uncertainty (S10).

### ACKNOWLEDGMENTS

J.C. acknowledges the China Scholarship Council (CSC), Grant No. 201603170247. I.E.Z., V.Z., and B.V. acknowledge the support from the ATTRACT project funded by the EC under Grant Agreement No. 777222. I.E.Z. acknowledges the support from the Nederlandse Organisatie voor Wetenschappelijk Onderzoek (NWO), LIFT-HTSM (Project No. 680-91-202). R.G. acknowledges support from the European Commission via the Marie Skłodowska-Curie Action Phonsi (Grant No. H2020-MSCA-ITN-642656). V.Z. acknowledges funding from the Knut and Alice Wallenberg Foundation grant “Quantum Sensors” and support from the Swedish Research Council (VR) through the VR Grant for International

Recruitment of Leading Researchers (Ref 2013-7152) and Research Environment (Grant No. Ref 2016-06122).

The authors declare no conflicts of interest.

### DATA AVAILABILITY

The data that support the findings of this study are available within the article and its [supplementary material](#).

### REFERENCES

- 1 C. Monroe, “Quantum information processing with atoms and photons,” *Nature* **416**, 238–246 (2002).
- 2 L.-M. Duan and H. Kimble, “Scalable photonic quantum computation through cavity-assisted interactions,” *Phys. Rev. Lett.* **92**, 127902 (2004).
- 3 M. D. Eisaman, J. Fan, A. Migdall, and S. V. Polyakov, “Invited review article: Single-photon sources and detectors,” *Rev. Sci. Instrum.* **82**, 071101 (2011).
- 4 Y. Liang, Q. Fei, Z. Liu, K. Huang, and H. Zeng, “Low-noise InGaAs/InP single-photon detector with widely tunable repetition rates,” *Photonics Res.* **7**, A1–A6 (2019).
- 5 W. Kang *et al.*, “Coincidence-pumping upconversion detector based on passively synchronized fiber laser system,” *IEEE Photonics Technol. Lett.* **32**, 184–187 (2020).
- 6 G. Gol’Tsman *et al.*, “Picosecond superconducting single-photon optical detector,” *Appl. Phys. Lett.* **79**, 705–707 (2001).
- 7 C. M. Natarajan, M. G. Tanner, and R. H. Hadfield, “Superconducting nanowire single-photon detectors: Physics and applications,” *Supercond. Sci. Technol.* **25**, 063001 (2012).
- 8 Y.-L. Tang *et al.*, “Measurement-device-independent quantum key distribution over 200 km,” *Phys. Rev. Lett.* **113**, 190501 (2014).
- 9 J. Yin *et al.*, “Satellite-to-ground entanglement-based quantum key distribution,” *Phys. Rev. Lett.* **119**, 200501 (2017).
- 10 S.-K. Liao *et al.*, “Satellite-to-ground quantum key distribution,” *Nature* **549**, 43–47 (2017).
- 11 S. Wengerowsky *et al.*, “Entanglement distribution over a 96-km-long submarine optical fiber,” *Proc. Natl. Acad. Sci. U. S. A.* **116**, 6684–6688 (2019).
- 12 H.-S. Zhong *et al.*, “12-photon entanglement and scalable scattershot boson sampling with optimal entangled-photon pairs from parametric downconversion,” *Phys. Rev. Lett.* **121**, 250505 (2018).
- 13 H. Wang *et al.*, “Boson sampling with 20 input photons and a 60-mode interferometer in a 10 14-dimensional Hilbert space,” *Phys. Rev. Lett.* **123**, 250503 (2019).
- 14 T. Zhong *et al.*, “Photon-efficient quantum key distribution using time-energy entanglement with high-dimensional encoding,” *New J. Phys.* **17**, 022002 (2015).
- 15 N. T. Islam, C. C. W. Lim, C. Cahall, J. Kim, and D. J. Gauthier, “Provably secure and high-rate quantum key distribution with time-bin qudits,” *Sci. Adv.* **3**, e1701491 (2017).
- 16 Z.-P. Li *et al.*, “Super-resolution single-photon imaging at 8.2 kilometers,” *Opt. Express* **28**, 4076–4087 (2020).
- 17 A. McCarthy *et al.*, “Kilometer-range, high resolution depth imaging via 1560 nm wavelength single-photon detection,” *Opt. Express* **21**, 8904–8915 (2013).
- 18 Y. Hochberg *et al.*, “Detecting sub-GeV dark matter with superconducting nanowires,” *Phys. Rev. Lett.* **123**, 151802 (2019).
- 19 A. Pe’er, Y. Bromberg, B. Dayan, Y. Silberberg, and A. A. Friesem, “Broadband sum-frequency generation as an efficient two-photon detector for optical tomography,” *Opt. Express* **15**, 8760–8769 (2007).
- 20 E. E. Wollman *et al.*, “Kilopixel array of superconducting nanowire single-photon detectors,” *Opt. Express* **27**, 35279–35289 (2019).
- 21 K. De Greve *et al.*, “Quantum-dot spin-photon entanglement via frequency downconversion to telecom wavelength,” *Nature* **491**, 421–425 (2012).
- 22 L. K. Shalm *et al.*, “Strong loophole-free test of local realism,” *Phys. Rev. Lett.* **115**, 250402 (2015).



- <sup>23</sup>M. Giustina *et al.*, “Significant-loophole-free test of Bell’s theorem with entangled photons,” *Phys. Rev. Lett.* **115**, 250401 (2015).
- <sup>24</sup>F. Marsili *et al.*, “Detecting single infrared photons with 93% system efficiency,” *Nat. Photonics* **7**, 210–214 (2013).
- <sup>25</sup>W. Zhang *et al.*, “NbN superconducting nanowire single photon detector with efficiency over 90% at 1550 nm wavelength operational at compact cryocooler temperature,” *Sci. China Phys., Mech. Astron.* **60**, 120314 (2017).
- <sup>26</sup>I. Esmaeil Zadeh *et al.*, “Single-photon detectors combining high efficiency, high detection rates, and ultra-high timing resolution,” *APL Photonics* **2**, 111301 (2017).
- <sup>27</sup>D. V. Reddy *et al.*, “Exceeding 95% system efficiency within the telecom C-band in superconducting nanowire single photon detectors,” in *CLEO: QELS\_Fundamental Science, FF1A-3* (Optical Society of America, 2019).
- <sup>28</sup>P. Hu *et al.*, “Detecting single infrared photons toward optimal system detection efficiency,” *Opt. Express* **28**, 36884–36891 (2020).
- <sup>29</sup>D. V. Reddy, R. R. Nerem, S. W. Nam, R. P. Mirin, and V. B. Verma, “Superconducting nanowire single-photon detectors with 98% system detection efficiency at 1550 nm,” *Optica* **7**, 1649–1653 (2020).
- <sup>30</sup>J. Zichi *et al.*, “Optimizing the stoichiometry of ultrathin NbTiN films for high-performance superconducting nanowire single-photon detectors,” *Opt. Express* **27**, 26579–26587 (2019).
- <sup>31</sup>B. Baek, A. E. Lita, V. Verma, and S. W. Nam, “Superconducting a-W<sub>x</sub>Si<sub>1-x</sub> nanowire single-photon detector with saturated internal quantum efficiency from visible to 1850 nm,” *Appl. Phys. Lett.* **98**, 251105 (2011).
- <sup>32</sup>S. Miki *et al.*, “Superconducting NbTiN nanowire single photon detectors with low kinetic inductance,” *Appl. Phys. Express* **2**, 075002 (2009).
- <sup>33</sup>J. K. W. Yang *et al.*, “Modeling the electrical and thermal response of superconducting nanowire single-photon detectors,” *IEEE Trans. Appl. Supercond.* **17**, 581–585 (2007).
- <sup>34</sup>L. You *et al.*, “Jitter analysis of a superconducting nanowire single photon detector,” *AIP Adv.* **3**, 072135 (2013).
- <sup>35</sup>J. Chang *et al.*, “Multimode-fiber-coupled superconducting nanowire single-photon detectors with high detection efficiency and time resolution,” *Appl. Opt.* **58**, 9803–9807 (2019).
- <sup>36</sup>H. Li *et al.*, “Multispectral superconducting nanowire single photon detector,” *Opt. Express* **27**, 4727–4733 (2019).
- <sup>37</sup>S. Miki, M. Yabuno, T. Yamashita, and H. Terai, “Stable, high-performance operation of a fiber-coupled superconducting nanowire avalanche photon detector,” *Opt. Express* **25**, 6796–6804 (2017).
- <sup>38</sup>H. Shibata, K. Fukao, N. Kirigane, S. Karimoto, and H. Yamamoto, “SNSPD with ultimate low system dark count rate using various cold filters,” *IEEE Trans. Appl. Supercond.* **27**, 1–4 (2016).
- <sup>39</sup>W. J. Zhang *et al.*, “Fiber-coupled superconducting nanowire single-photon detectors integrated with a bandpass filter on the fiber end-face,” *Supercond. Sci. Technol.* **31**, 035012 (2018).
- <sup>40</sup>S. N. Dorenbos *et al.*, “Superconducting single photon detectors with minimized polarization dependence,” *Appl. Phys. Lett.* **93**, 161102 (2008).